Deciphering groundwater potential zones of Sarenga block, West Bengal, India using Geographic Information System and Multi-Criteria Decision-Analysis methods

Suraj Dule[1] , **Arabinda Sharma*[2]**

[1]*Gangadhar Meher University, PhD Scholar, School of Geography, Sambalpur, India, Email:suraj.dule@gmail.com*
[2]Gangadhar Meher University, Associate Professor, School of Geography, Sambalpur, India, Email:arbind_78@rediffmail.com

Abstract

The increasing demand for water in recent decades has led to continuous exploitation and mismanagement of groundwater resources worldwide. This has often resulted in the reduction of the water table and deterioration of water quality due to non-sustainable consumption and excessive extraction practices. To address these issues, it is very crucial to analyse Groundwater Potential (GWP) zones periodically. In this study, Geographic Information System (GIS) and Remote Sensing (RS) techniques coupled with Analytical Hierarchy Process (AHP), Multi Influencing Factor (MIF), and Random Forest (RF) algorithm have been used to define GWP zones. These methods helped to identify, weigh, and rank eleven major hydrogeological factors influencing groundwater potential (GWP). A novel application of the RF algorithm utilized to generate high-resolution GWP maps outperformed AHP (0.875) and MIF (0.828) with a Receiver Operating Characteristic (ROC) of 0.982 in GWP delineation, as assessed by the Area Under the Curve (AUC) analysis. The outcome from AHP, MIF, and RF methods revealed that around 60-70% of the study area showed poor to fair GWP while only 30- 40% of the area exhibited good to excellent GWP. The results revealed that a significant portion of the study area exhibits poor to fair GWP, highlighting the urgent need for sustainable GW management strategies. These findings provide valuable insights for policymakers and local farmers to make informed decisions on sustainable GW management plans tailored to the specific needs of the study area.

1. Introduction

Humanity relies on water for drinking and carrying out daily activities, making it essential for the evolution of human civilization. The significant rise in the global population over the past few decades has created a large demand for the world's available freshwater supplies [1-2]. To address this increasing water demand, groundwater has been identified as one of the key sources of freshwater for domestic, industrial, and agricultural uses [3]. In developing countries like India, where approximately 65% of its population depends on agriculture, the accessibility and reliance on groundwater play a crucial role for living [4-5]. Consequently, the growing demand for groundwater, coupled with inadequate governance to manage it, has led to the over-exploitation of groundwater in various parts of the country, reducing groundwater levels and contributing to the water crisis [6].

In addition to over-exploitation, human-induced land use changes, erratic rainfall patterns, etc. remarkably influence groundwater availability [7-8]. Furthermore, hard rock formations limit groundwater accessibility due to their sparse pore spaces, which restrict water movement [9]. Addressing these challenges requires sustainable groundwater management techniques, particularly in countries like India. Effective monitoring and management of groundwater resources can be achieved through groundwater potential (GWP)

zone mapping using Geographic Information Systems (GIS) and remote sensing (RS) techniques [10]. These technologies integrate geographical data collected at different spatial and temporal scales to assess groundwater recharge potential and inform decision-making [11]. GIS and RS can quickly help in problem-solving in real-world situations by providing high-resolution satellite datasets with higher accuracy along with efficiency in saving time and cost. GIS and RS coupled with Multi-Criteria Decision Analysis (MCDA), statistical models, and machine learning (ML) techniques can efficiently identify GWP zones as well as other risk areas [12-13]. These methods streamline the process, reduce time and costs, and maintain high accuracy by evaluating various factors that influence groundwater potential (GWP), and assigning ranks and weights based on their impact [14]. Common MCDA techniques include Analytical Hierarchy Process [15-17], Multi-Influencing Factor [18-19], Random Forest [20-22], Frequency Ratio [19,23], and Drastic method [24].

In the assessment of GWP at micro-planning levels such as blocks, prior studies have primarily focused on larger geographical areas like districts, states, or large river basins. These studies commonly rely on secondary data for easier validation and higher accuracy, despite challenges posed by data scarcity from low-resolution RS imagery and inadequate meteorological data [25]. Notably, NRSC ISRO used LISS-III datasets with a resolution of 23.5 m in 2011 to carry out their most recent authorized mapping of GWP zones in the research area.

The study area considered in this work has a long history of water scarcity, accompanied by groundwater-dependent poor agricultural practices and increasing population pressure capability have led to a high demand for water against its lesser availability. Therefore, there is a keen need for a highly equipped strategy to cope with these challenges and effectively bridge the gap between water availability and demand. In order to achieve this target, identifying the potential zones of groundwater availability and its proper management is highly recommended which can only be achieved through modelling the GWP using proper statistical and GIS-based techniques [26]. The present work has employed three widely recognized methodologies, Analytical Hierarchy Process (AHP), Multi Influencing Factor (MIF), and Random Forest (RF), to identify the GWP in the Sarenga block of Bankura district, West Bengal in India. It also has attempted to perceive the best method suitable for delineating the GWP. This study integrated various physio-climatic factors derived from RS datasets and ancillary datasets, such as geomorphology, geology, rainfall, drainage, soil topography, land use and land cover (LULC) and groundwater level data within the three methods to understand their role in groundwater potential and its variability in the study area. The outcome of this data-driven approach tailored to Sarenga's unique hydrogeological setting will help in micro-level planning and management of groundwater. The insights gained contribute to a more sustainable approach to groundwater management, aligning local groundwater potential with regional conservation and land management, resource planning goals, and agricultural applications using GIS and Remote sensing in areas with similar hydrogeological set-ups.

2. Method

2.1 Study Area

The current research focuses on the Sarenga development block in the Bankura district of West Bengal shown in Figure 1. Geographically, it is situated between $86^0 55'37''$ E to $87^0 44'20''$ E and $22^0 38'55''$ N to $22^0 54'27''$ N, encompassing an area of approximately 224 km². Sarenga is bordered by Raipur block to the west, Simlapal block to the north and northeast, and West Medinipur district to the south and southeast. The region experiences an average annual rainfall of about 1386 mm. Topographically, the terrain is highly dissected, with an average slope of approximately 10–20 m/km. Geologically, it features lateritic and older alluvium strata from the Pleistocene era, supporting groundwater in confined to semi-confined states. Drilled wells in the area are typically 10 to 15 meters deep and 3 meters in diameter [27]. The land is drained by the Kansabati River on its western side, an area with promising agricultural prospects. In contrast, the eastern side lacks a reliable water supply for irrigation and depends on seasonal rain, canals, and groundwater. Sarenga block along with the whole Bankura district has witnessed population growth, modernization of agricultural activities, and urbanization in past two decades. Despite the expansion of economic development and employment opportunities, challenges in sustainable groundwater management, climate adaptation, and future resilience persist. The Rajiv Gandhi National Groundwater Mission had played a pivotal role in afforestation, enhanced irrigation, and modern farming methods for improving groundwater management. According to Central Ground Water Board's (CGWB) report 2022 [28], these initiatives have benefited crops such as paddy and maize, reducing dependency on monsoon rains in the study area.
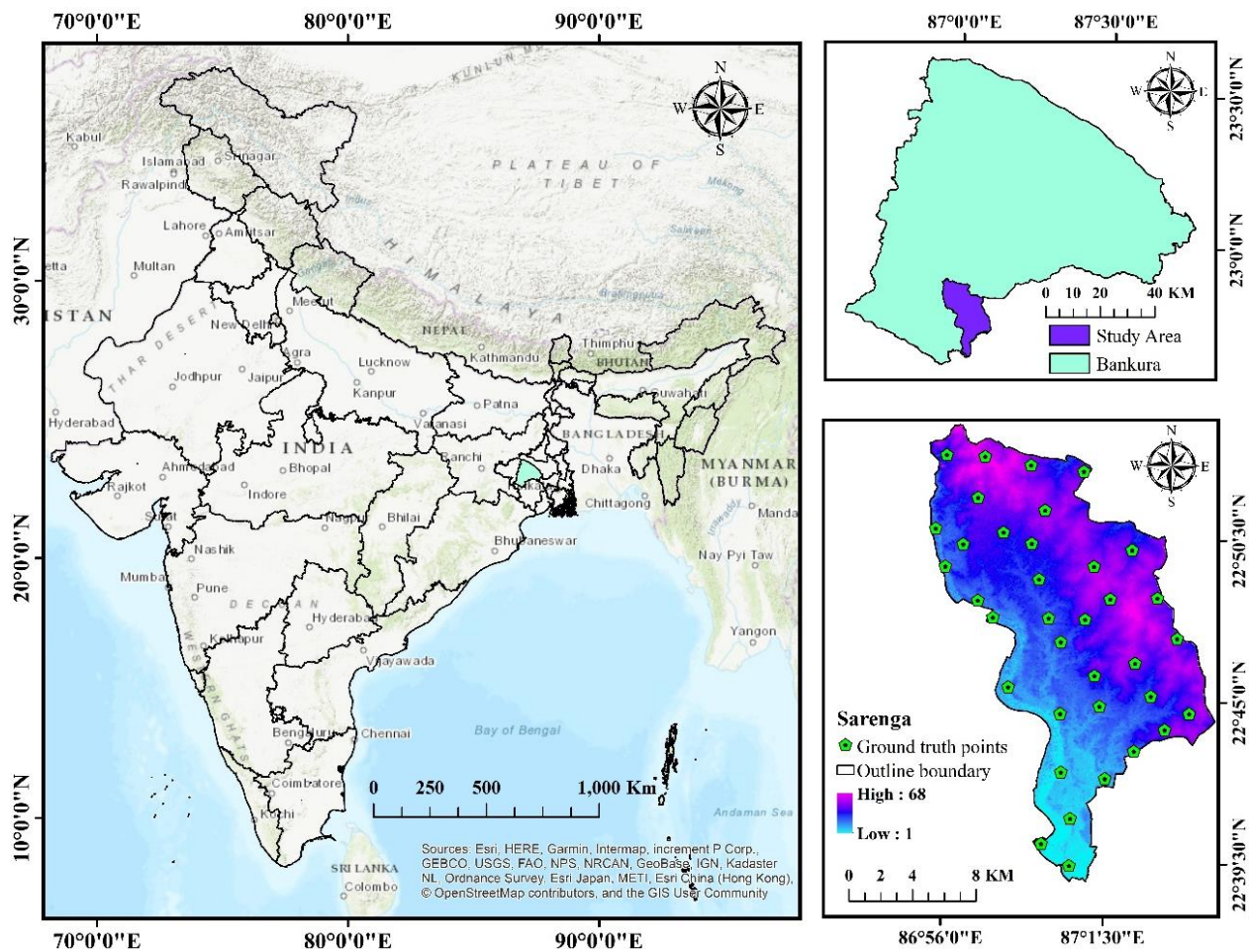
Figure 1. Location map of the Sarenga development block

2.2 Material Sources

The study area's base map was created using a 1:50,000 scale topographic map (73 J/13, 73 J/14, 73 N/1, and 73 N/2) obtained from the Survey of India (SOI). Eleven physio-climatic factors contributing to the Groundwater (GW) recharge were selected. Some of them were obtained from RS imageries like drainage density (DD), lineament density (LD), slope (SL), land use and land cover (LULC), and the topographic wetness index (TWI), while some of the datasets obtained either in grided, image and vector form, which were later digitized and processed in GIS environment to be used in this work like geomorphology (GM), geology (GG), rainfall (RF), soil texture (ST), pre-monsoon and post-monsoon water levels (WL PRM & WL PM). Data for these factors were collected from secondary sources, processed, and converted into raster layers using QGIS. The GM map was created from Bhukosh GSI maps at a 1:250,000 scale and refined with a groundwater prospect map from NRSC ISRO. The GG map was based on the Geological Survey of India's district resource map at the same scale. RF data ranging from 1901 to 2022, obtained from the Indian Meteorological Department (IMD) Pune, were assessed to create the rainfall map. DD, LD, SL, and TWI maps were derived from ALOS PALSAR DEM data obtained from the Alaska Satellite Facility with

a resolution of 12.5 x 12.5 meters. The ST map was digitized from the ICAR NBSS and LUP's data of Bankura district. Additionally, the Sentinel-2 satellite image for the year 2022 was utilized to develop the LULC map which was subsequently validated using the Kappa-coefficient. Groundwater level fluctuation maps for pre- and post-monsoon periods were created using 2022 data from Water Resource Information System managed by Central Ground Water Board, India. Finally, actual groundwater (GW) yield data for validation were obtained from a 1:50,000 scale groundwater prospect map prepared by NRSC ISRO in 2022 using regional average annual ground truth observation, and available on the West Bengal Public Health Engineering Department portal.

2.3 Methods

The methodologies used in this study are depicted with the help of a flowchart in Figure 2. Some important methods applied in this study are briefly discussed.

2.3.1 Lineament and Drainage Density Map

The lineament and drainage density for the study region were prepared using the RS dataset in the form of ALOS PALSAR DEM acquired from the Alaska

Satellite Facility in QGIS. The following formulas have been used to calculate the (L_d) lineament density [29] and (D_d) drainage density:

$$L_d = \frac{\sum_{i=1}^{n}(L_i)}{A}, \tag{1}$$

$$D_d = \frac{\sum_{i=1}^{n}(D_i)}{A}, \tag{2}$$

where $\sum L_i$ = sum of all the lineament length in kilometer, $\sum D_i$ = total of all stream lengths in km, and A = Area in km^2.

2.3.2 Analytical Hierarchy Process (AHP)

The AHP technique evaluates multiple elements based on their relative importance using expert knowledge from literature reviews [30-31]. It assigns weights and ranks to parameters, creating an eigenvalue pairwise comparison matrix. The rank and weight of each parameter are determined by its relative importance to others, assessed using Saaty's absolute scale from 1 to 9, where 1 indicates equal importance and 9 indicates extreme importance [32]. This scale constructs the pairwise matrix (Table 1) and the normalized pairwise matrix using the following equation:

$$Nij = \frac{Iij}{\sum Ij}, \tag{3}$$

where Nij represents the normalized cell value for each cell, Iij is the individual cell weight, $\sum Ij$ is the total weight of the corresponding column in that cell.

Normalized weights are calculated from the normalized pairwise matrix by using the following formulae:

$$Nw = \frac{\sum Nij}{n}, \tag{4}$$

where Nw denotes the normalized weight of each parameter, $\sum Nij$ indicates the sum of normalized weights of the row and represents the number of factors analyzed.

Following the creation of a normalized pairwise matrix, the Consistency Ratio (CR) and Index (CI) were computed, with the following equations:

$$CR = \frac{CI}{RI}, \tag{5}$$

where RI for Randomness Index.

$$CI = \frac{\lambda max - n}{n-1}, \tag{6}$$

where λ_{max} denotes the principal eigenvalue and n represents the number of factors considered. The results are derived using the mentioned formulas.
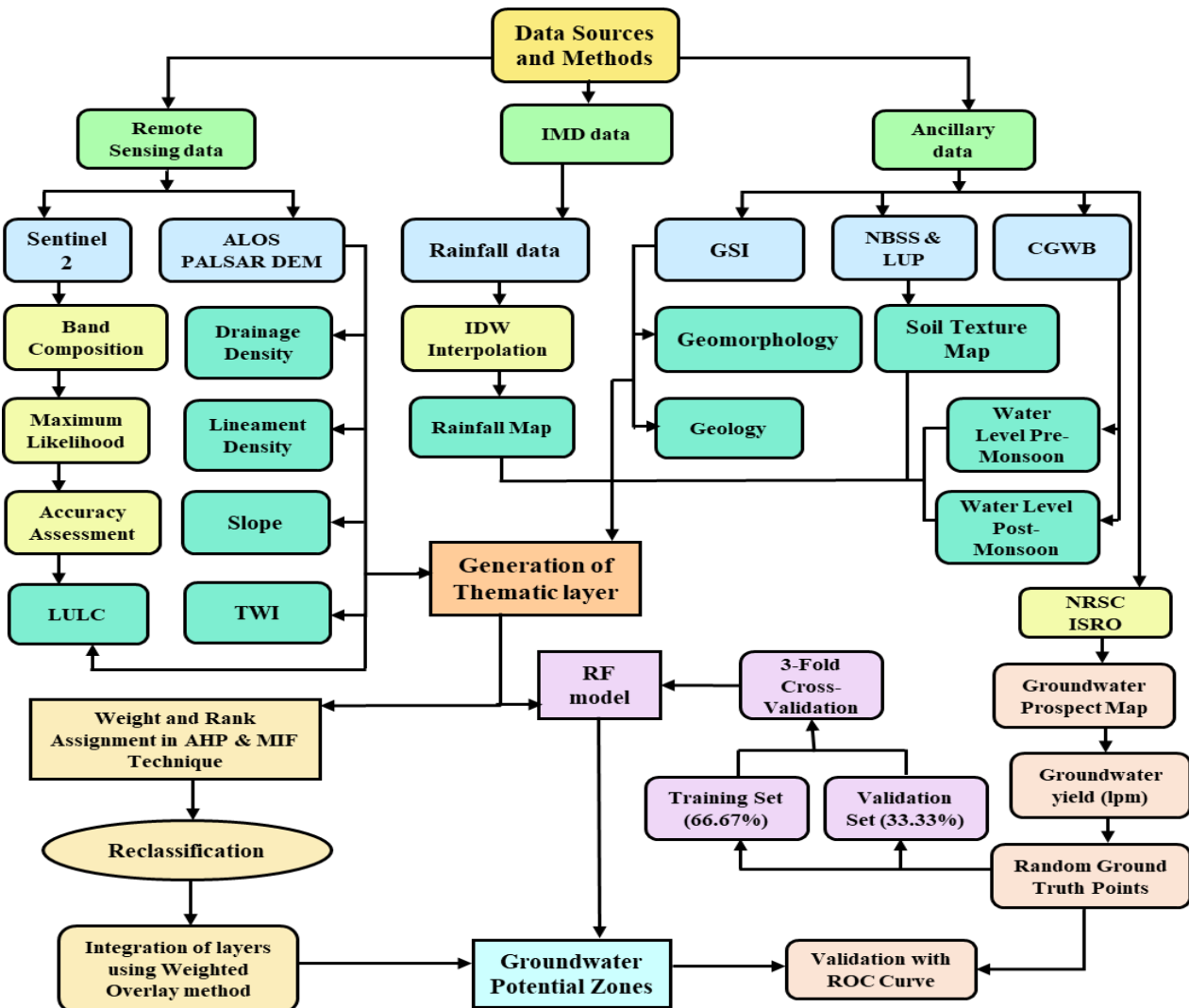

Figure 2. Flow chart of methodologies adopted for groundwater potential zone mapping.

Table 1. Pairwise comparison matrix table for AHP

Factors	GM	GG	RF	DD	LD	ST	SL	LULC	WL PRM	WL PM	TWI
GM	1	2	3	2	2	3	3	6	6	5	4
GG	1/2	1	2	3	2	4	3	2	6	5	5
RF	1/3	1	1	3	3	3	4	3	5	5	5
DD	1/2	1/3	1/3	1	3	4	4	2	4	3	4
LD	1/2	1/2	1/3	1/3	1	4	4	2	4	5	2
ST	1/3	1/4	1/3	1/4	1/4	1	2	3	3	3	2
SL	1/3	1/3	1/4	1/4	1/4	1/2	1	2	3	2	3
LULC	1/6	1	1/3	1/2	1/2	1/3	1	1	3	2	2
WL PRM	1/6	1/6	1/5	1/4	1/4	1/3	1/3	1/3	1	1	3
WL PM	1/5	1/5	1/5	1/3	1/5	1/3	1/2	1/2	1	1	4
TWI	1/4	1/5	1/5	1/4	1/2	1/2	1/3	1/2	1/3	1/4	1
Sum	4.28	5.98	8.18	11.17	12.95	21.00	22.67	22.33	36.33	32.25	35.00

2.3.3 Multi Influencing Factor (MIF)

The MIF approach is an MCDA method where various influencing factors are evaluated based on their mutual relationships and impact strengths. Factors with significant influencing capability are assigned a score of 1, while those with moderate to low influence are assigned with 0.5. Conversely, higher scores indicate stronger influencing capabilities. The proposed value of a factor is determined by aggregating all significant and moderate effects (18). Table 2 presents the assigned scores for all parameters in this study. The following equation computes the cumulative score for each parameter:

$$Introduced\ Score = \frac{A+B}{\sum(A+B)} \times 100, \qquad (7)$$

where A represents the significant influence between two parameters, while B denotes the minor influence between them. Figure 3 illustrates the relative interdependence among the multiple influencing factors.
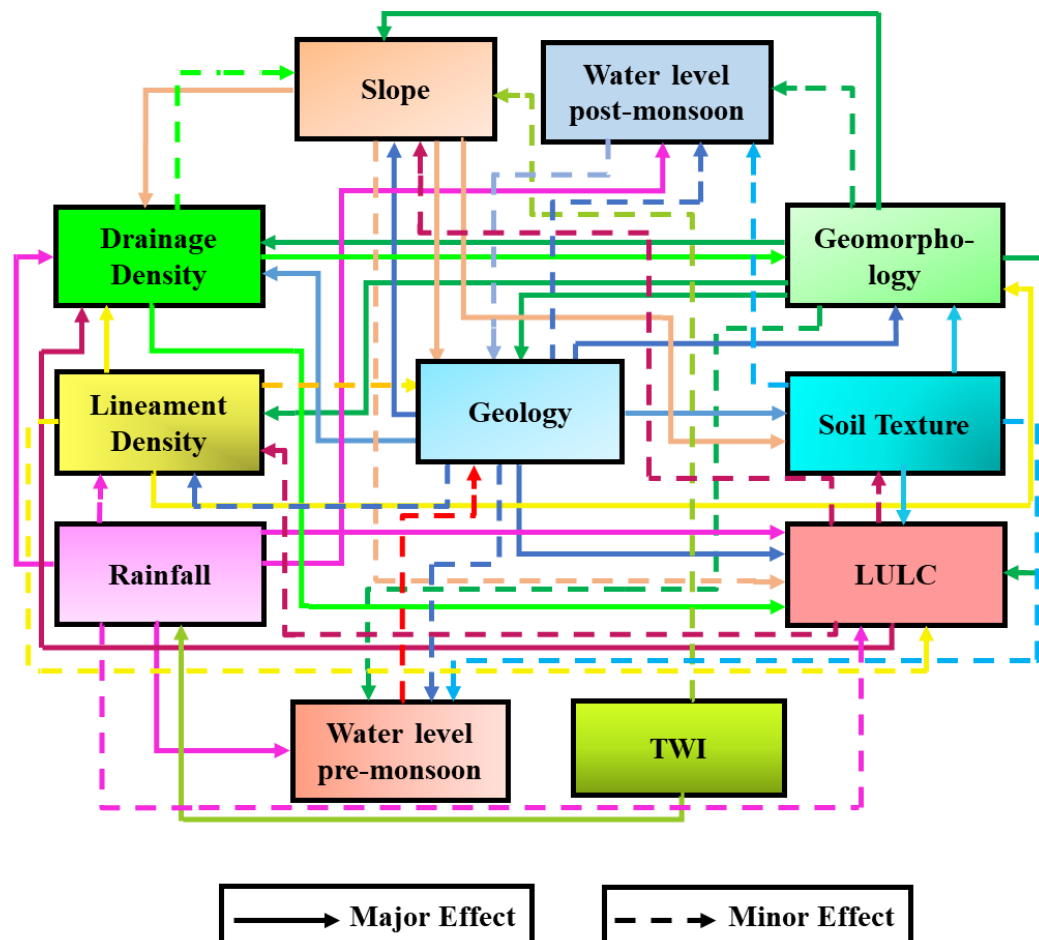

Figure 3. The flowchart outlines the inter-relationship between all the influencing factors and their effects

Table 2. Major and minor effects for obtaining introduced score in MIF

Factors	Major Effect (A)	Minor Effect (B)	Proposed Value (A + B)	Assigned Score
GM	1 + 1 + 1 + 1 + 1 + 1	0.5 + 0.5	7	19
GG	1 + 1 + 1 + 1 + 1	0.5 + 0.5 + 0.5	6.5	18
RF	1 + 1 + 1 + 1 + 1	0.5 + 0.5 + 0.5	5.5	15
DD	1 + 1	0.5	2.5	7
LD	1 + 1	0.5 + 0.5	3	8
ST	1 + 1	0.5 + 0.5	3	8
SL	1 + 1 + 1	0.5	3.5	10
LULC	1 + 1	0.5	2.5	7
WL PRM		0.5	0.5	2
WL PM		0.5	0.5	2
TWI	1	0.5	1.5	4
Sum			36	100

2.3.4 Random Forest (RF)

The RF model enhances accuracy and reduces overfitting by aggregating multiple decision trees trained on random data subsets [33]. It is effective for both classification and regression tasks, capable of estimating feature importance and handling noisy datasets, making it ideal for GWP assessment. Despite its computational demands, it offers robust performance and interpretability, although it may be less precise than complex models like gradient boosting machines or neural networks [34]. Notably, RF excels in analysing intricate spatial relationships in hydrogeological studies [33, 35].

The Google Colab open-sourced Python API was used to facilitate the GWP map creation using RF model. For supervised learning, we utilized a feature class with categorized GWP points, mapped to numerical values (from 'excellent' as 0 to 'poor' as 3). Raster values were extracted to form a feature matrix (X_train), with labels (y_train) derived from ground truth data shapefile. To optimize the model, tuning parameters such as the number of trees (n_estimators), tree depth (max_depth), and min_sample_leaf, min_samples_split have been employed. GridSearch Cross-Validation (using cross_val_predict) validated the model's performance through confusion matrices and classification reports [36-38]. The best-performing configuration included n_estimators=200, max_depth=None, min_samples_leaf=1, and min_samples_split=2.

A three-fold cross-validation with 36 random points ensured robust performance estimates. The RF model achieved an overall classification accuracy of 78%. Class-wise precision, recall, and F1-scores were highest for 'excellent' and 'poor' GWP zones, indicating strong discriminative performance. Finally, the trained RF model predicted GWP classes across the entire study area.

2.3.5 GWP maps in AHP and MIF

Integrating all thematic layers created from the RS and ancillary datasets is vital for GWP demarcation before doing that, the digitization and reclassification of these layers is a significant need in the zonation process which was exclusively done in the QGIS environment. To ensure uniformity, all raster layers were resampled to the same pixel size. The appropriate weights were assigned to each thematic layer as shown in Table 3, and each sub-class of the layers was given a suitable rank.

Table 3. Parameters weightage in AHP and MIF method

Factor	Parameter	AHP weight	MIF weight	GWP	Rank
GM	Lateritic Plain - Lithomarge Clay	20	19	Fair	5
	Dissected Lateritic Upland			Poor	3
	Granitoid Gneiss -Valley Fill Shallow			Good	7
	Alluvium Plain Young - sand and silt			Excellent	8
	Alluvium Channel Bar - Sand Dominant			Excellent	9
	Alluvium Plain Older - sand, silt and clay			Good	7
	Laterite - Valley Fill Shallow			Fair	5
GG	Laterite	17	18	Fair	5
	Sand, silt and clay			Good	6
	Clay impregnated with caliche			Good	7
	Sand and silt			Good	6
	Alternating layers of sand, silt and clay			Excellent	9

	Newer alluvium			Good	7
	Mica schist, occasionally garnet ferrous			Good	6
RF (mm)	1305 - 1321	15	15	Fair	5
	1321 - 1330			Good	6
	1330 - 1337			Good	7
	1337 - 1344			Excellent	8
	1344 - 1351			Excellent	9
DD (km/km^2)	0 - 1.51	12	7	Fair	5
	1.51 - 3.28			Good	6
	3.28 - 5.05			Good	7
	5.05 - 7.27			Excellent	8
	7.27 - 12.92			Excellent	9
LD (km/km^2)	0 - 0.31	10	8	Poor	3
	0.31 - 0.81			Poor	3
	0.81 - 1.28			Fair	4
	1.28 - 1.84			Fair	5
	1.84 - 3.14			Good	6
ST	Waterbody	6	8	Excellent	9
	Gravelly sandy clay-Clay loam to sandy clay loam			Fair	5
	Clay loam to clay-Clay			Fair	4
	Sandy-Loamy sand to sandy loam			Excellent	8
	Gravelly sandy loam-Gravelly sandy loam			Good	6
	Sandy clay loam-Clay loam to sandy clay loam			Good	7
	Sandy clay loam to sandy clay			Fair	5
	Sandy loam to clay loam-Gravelly sandy clay			Excellent	8
SL (degree)	0 - 1.35	5	10	Excellent	8
	1.35 - 3.37			Good	7
	3.37 - 5.23			Good	6
	5.23 - 7.84			Fair	5
	7.84 - 20.15			Fair	4
LULC	Built-up area	5	7	Poor	3
	Vegetation			Excellent	8
	Agriculture			Excellent	9
	Waterbody			Excellent	9
	Bare land and sand			Fair	4
WL PRM (mbgl)	6.58 - 7.67	3	2	Good	7
	7.67 - 8.46			Good	6
	8.46 - 9.44			Fair	5
	9.44 - 10.57			Fair	4
	10.57 - 11.90			Poor	3
WL PM (mbgl)	2.34 - 2.80	4	2	Excellent	9
	2.80 - 3.17			Excellent	8
	3.17 - 3.50			Good	7
	3.50 - 3.89			Good	6
	4.89 - 4.43			Fair	5
TWI	3.56 - 6.58	3	4	Fair	4
	6.58 - 8.43			Fair	5
	8.43 - 10.56			Good	6
	10.56 - 13.44			Excellent	8
	13.44 - 21.05			Excellent	9

Finally, a weighted overlay analysis using the following formulae was performed to integrate all thematic layers and generate the GWP map for the study region:

$$GWP = \sum_{i=1}^{n}(M_i \times N_i), \tag{8}$$

Where, GWP stands for Groundwater Potential, n is the number of influencing factors, M_i is the

thematic layer weight, N_i is the thematic layer rank and i represents every influencing factor considered.

2.3.6 Data Limitation

Despite rigorous data preparation and validation, still there are possibility of some uncertainties and limitations. DEM-derived layers (slope, drainage density, lineament density, and TWI) may carry vertical and horizontal errors that affect derived indices. Rainfall interpolation using IDW, based on a moderate density of IMD stations, may not fully capture localized variability. Geology and soil texture maps (1:250,000 scale) may underrepresent fine-scale heterogeneity, while the Sentinel-2 LULC layer is subject to seasonal and classification uncertainties. Groundwater level data were restricted to 2022, limiting temporal assessment. These uncertainties are common in GIS-based hydrogeological studies but were minimized through resolution standardization and robust validation. Future studies should integrate multi-temporal datasets, denser observations, and ensemble modelling to enhance reliability.

3.   Results and Discussions

3.1 Geomorphology (GM)

The geomorphology of an area plays a crucial role in identifying potential groundwater zones. The structure and lithological properties of different landforms, which greatly influence groundwater availability of the region, is presented in Figure 4.

Figure 4. Geomorphology map (**Lp**-Lateritic plain, **Lc**-Lithomarge clay, **Dlp**-Dissected lateritic plain, **Gg**-Granitoid gneiss, **Vfs**-Valley fill shallow, **Apy**-Alluvium plain young, **s & s**-sand and silt, **Acb**-Alluvium channel bar, **sd**-sand dominant, **Apo**-Alluvium plain older, **c**-clay, **L**-laterite).

Geomorphological factors also play a significant role in determining the infiltration rate and volume of water present underground inside a specific location [30,39]. For instance, the lateritic plain with lithomarge clay (12.8%) has respectable groundwater potential due to its intermediate permeability, allowing for some infiltration but limited storage. On the other hand, steep slopes in the dissected lateritic upland (22.3%) increase runoff and reduce infiltration, resulting in low groundwater recharge. In the north and east, the shallow granitoid gneiss valley fills (7.4%) offer high potential, especially near rivers where weathered zones improve storage and transmission. Similarly, the young alluvium plains (18.1%) with sand and silt have high permeability, aiding effective infiltration and recharging. In contrast, the alluvium channel bar with sand dominance (6.2%) shows strong groundwater potential due to good infiltration and storage capacity, whereas the older alluvium plains (8.4%) near rivers are promising for storage and recharging. Understanding the geomorphological characteristics is crucial for effective groundwater resource management [40-41].

3.2 Geology (GG)

The presence of groundwater in an area is greatly affected by its geological composition, which affects the porosity and permeability of the rock. The rocks exposed on the surface play a crucial role in determining the likelihood of groundwater presence in an area [9,42-43].
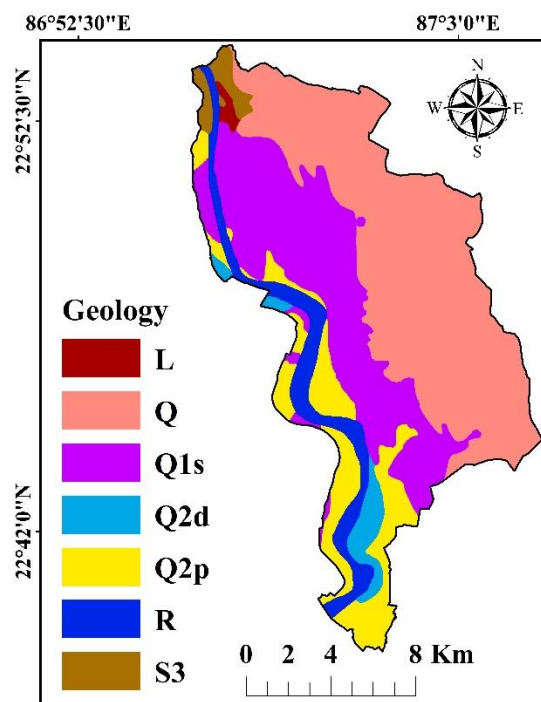

Figure 5. Geology map (**L**-Laterite, **Q**-Sand, silt and clay, **Q1s**-Clay impregnated with caliche, **Q2d**-Sand

and silt, **Q2p**-Alternating layers of sand, silt and clay, **R**-River, **S3**-Mica schist occasionally garnetiferrous).

The various geological units of the study area have a differential impact on its groundwater potential due to their varying composition and properties (Figure 5). In the northern area, laterite (0.5%) has fair groundwater potential due to moderate permeability, allowing some infiltration but with limited storage. The extensive zone of sand, silt, and clay (44.9%) offers good potential due to mixed grain sizes, facilitating both infiltration and storage. Clay containing caliche (28.8%) creates confined aquifers, enhancing groundwater storage. The sand and silt zone (2.9%) has good potential due to high permeability, promoting efficient recharge. New alluvium (7.9%) allows high infiltration rates and substantial storage. Mica schist (2.1%) in various regions offers good potential due to its foliated structure, storing and transmitting groundwater via fractures. Alternating layers of sand, silt, and clay (12.9%) in the south and west have excellent potential due to multiple aquifer systems [44-45].

3.3 Lineament Density (LD)

LD are geological features such as rock structures, joints, faults, and folds that help water quickly seep into the subsurface and thus directly influence the groundwater potential. This layer was created using the remotely sensed ALOS PALSAR DEM. The area was categorized into five LD classes given in Figure 6.

Figure 6. Lineament density map.

Areas with LD ranging from 0 - 0.31 km/km² (33.7%) and 0.31 - 0.81 km/km² (22.3%) are

categorized as poor, 0.81 - 1.28 km/km² (27.9%) and 1.28 - 1.84 km/km² (10.7%) as fair, and 1.84 - 3.14 km/km² (5.4%) as having good groundwater potential zones. Areas having high LD typically have strong groundwater potential, and vice-versa. Studies have also shown that lineaments can serve as pathways for groundwater flow, especially in fractured rock aquifers, improving the storage and movement of groundwater [46]. High LD can also suggest the presence of extensive fracture networks, which are important for groundwater movement and storage in hard rock terrains [47].

3.4 Drainage Density (DD)

DD is inversely related to aquifer permeability and infiltration rate, making it crucial in determining the groundwater potential of a location [48]. High DD of a location symbolizes greater surface runoff and reduced infiltration, resulting in low groundwater potential, while low DD enhances infiltration, leading to high groundwater potential [49-50]. The DD values of the study area ranging between 0 to 1.51 km/km² (27.9 percent) have been considered as fair, 1.51 - 3.28 km/km² (27.4 percent), and 3.28 - 5.05 km/km² (23.5 percent) as good, and 5.05 - 7.27 km/km² (16.2 percent) and 7.27 - 12.92 km/km² (5 percent) considered as the zones of excellent groundwater prospects.
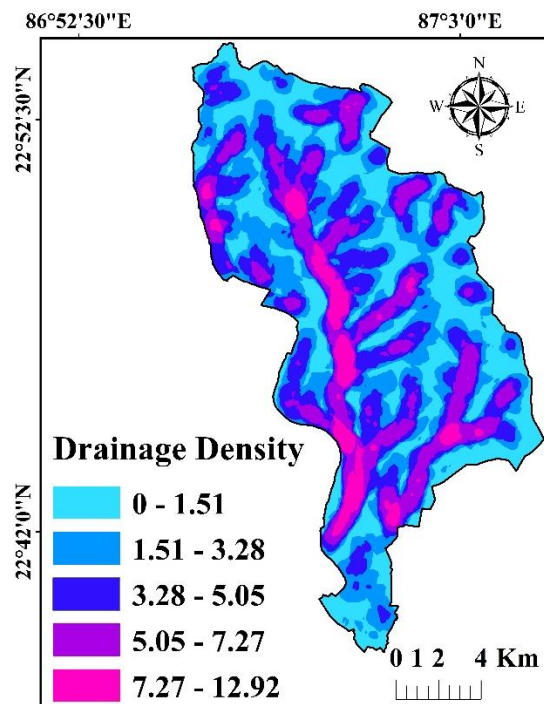

Figure 7. Drainage density map.

High DD is often associated with less permeable surfaces that hinder water from percolating into the ground, reducing groundwater recharge [51]. This study has effectively revealed that the central and western parts of the study area have high DD, while the eastern and northern parts have comparatively lower DD, which are shown in Figure 7.

3.5 Water Level Pre and Post-Monsoon (WL PRM and PM)

It is important to understand water level fluctuations below ground to assess groundwater potential. Data from the India-WRIS portal for 2022 was processed into a raster layer. Typically, during the arrival of monsoon season (July-September), the rise in water levels and saturation of the aquifers can be observed. This study has successfully portrayed a decreasing trend in water levels from southwest to northeast during both the pre-monsoon and post-monsoon periods which has been depicted in Figure 8 and Figure 9.

Figure 8. Pre-monsoon water level map.

Areas with varying post-monsoon water levels have been classified into five categories, the water level between 2.34 - 2.80 meters below ground level (mbgl) (3.9 percent) and 2.80 - 3.17 mbgl (10 percent) has been classified as excellent, 3.17 - 3.50 mbgl (33.1 percent) and 3.50 - 3.89 mbgl (32.2 percent) named as good, and 3.89 - 4.43 mbgl (20.8 percent) as fair groundwater potential zones. Increased precipitation and surface runoff during this period significantly enhance groundwater rechargeability [52].

On the other hand, the pre-monsoon period experiences declining water levels due to reduced or negligible rainfall over months. This dry season leads to a region-wide drop in groundwater levels. Pre-monsoon water levels also vary across the whole study area, which further classified as good prospect zone with range 6.58 - 7.67 mbgl (24.8 percent) and 7.67 - 8.46 mbgl (31 percent), fair prospect zone between 8.46 - 9.44 mbgl (18.6 percent) and 9.44 - 10.57 mbgl (14.8 percent), and the poor potential areas with water level range 10.57 - 11.90 mbgl (10.8

percent) stressing the need for effective groundwater management.
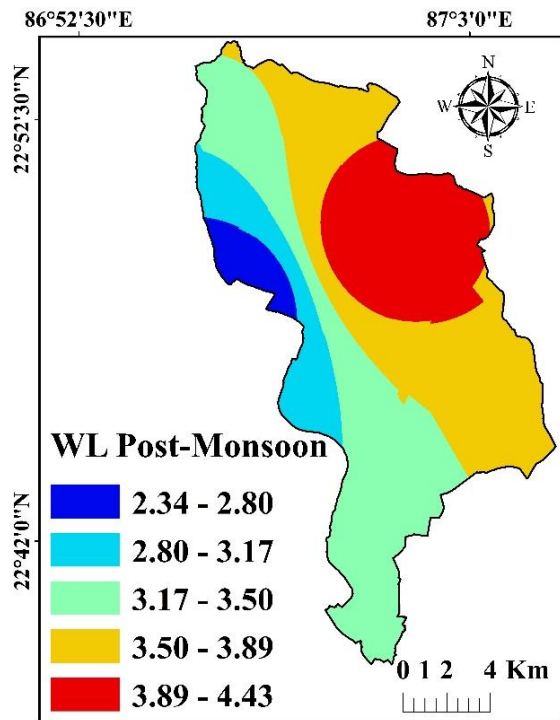

Figure 9. Post-monsoon water level map.

3.6 Rainfall (RF)

Rainfall is the primary natural water source, influencing groundwater replenishment by infiltrating rock fissures and porous spaces. Areas with higher rainfall generally exhibit greater groundwater potential, contrasting with regions receiving less rainfall. Consistent and substantial rainfall raises soil moisture levels and maintains a steady recharge rate, essential for sustaining groundwater levels.

Conversely, areas with little rainfall may experience reduced recharge rates, resulting in lower groundwater levels and potential depletion over [29,53]. According to IMD Pune rainfall data, the annual rainfall in the study area varies from 1305 to 1351 mm [54]. A rainfall layer was created using the IDW method and categorized into five classes based on spatial distribution (see Figure 10). IDW was specifically chosen due to its simplicity, computational efficiency, and suitability for areas with limited or moderately spaced stations. It assumes that closer points exert greater influence on interpolation, which aligns with the spatial rainfall pattern of the study area [15,48]. The rainfall layer revealed that the rainfall intensity gradually decreases from southwest to northeast. Further five rainfall classes have been created where the areas receiving 1305 to 1321 mm (9.7 percent) had fair prospect, 1321 to 1330 mm (15.9 percent), 1330 to 1337 mm (26.5 percent) as good, and 1337 to 1344 mm (39 percent), and 1344 to 1351 mm (8.9 percent) as excellent GWP.
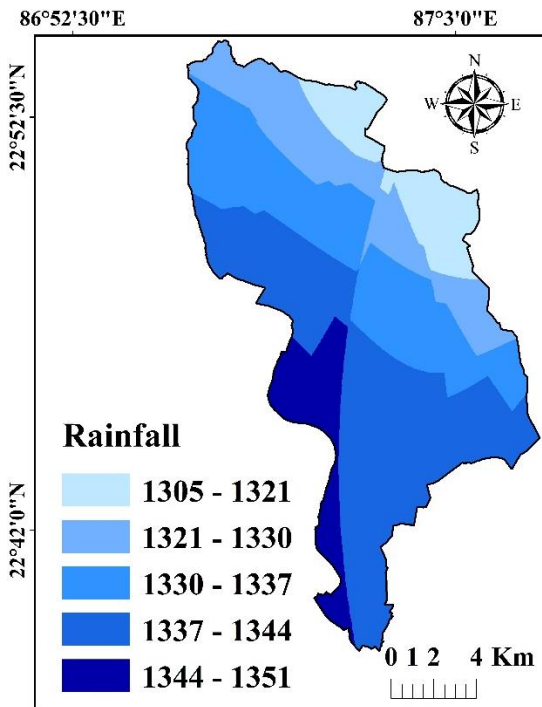
Figure 10. Rainfall map.

Figure 11. Land use and land cover map.

3.7 Land Use and Land Cover (LULC)

As the land use and land management strategies directly influences the infiltration, percolation, and overland flow, and aids in the restoration of GWP, land use and land cover (LULC) play a significant role in the groundwater recharge procedure. It reflects the various natural and man-made features that cover the surface of the ground, as well as how humans use the land [55-57]. This study examines a range of LULC parameters and their fluctuating effects on groundwater potential within the study area. In summary, five LULC classes are taken into consideration for this study. Following the creation of the LULC map of 2022, these classes were verified using Google Earth Pro to match the ground truth actuality (Figure 11). Of the 220 random points that were generated for the accuracy testing of the final map, 203 points in total accurately represent the LULC groupings based on the ground truth data [58-59]. The built-up areas covering 1.5% of the total area have a low groundwater prospect (GWP) due to their impermeable surfaces that hinder infiltration. A fair GWP with moderate infiltration has been found in the areas with bare soil and 12.0% sand cover. Vegetation (24.3%) and agricultural regions (60.5%) have high GWP because of the improved infiltration and recharge governed about by plant roots and soil structure [48]. Waterbodies (1.7%) provide direct recharge zones, which is considered as an excellent prospect.
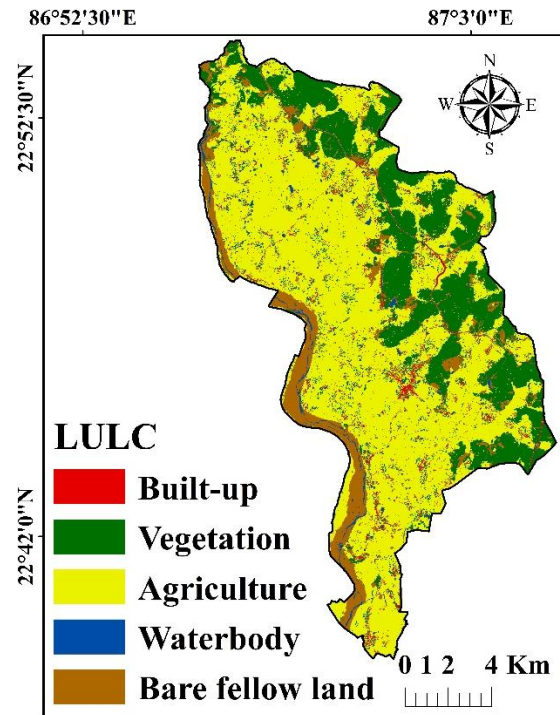
3.8 Slope (SL)

The slope of a landform denotes its tilt or gradient relative to a horizontal surface. This parameter influences GWP by affecting surface runoff and infiltration rates. Slope gradient significantly impacts rainfall distribution, surface runoff, and infiltration rates, thereby influencing groundwater retention [60].
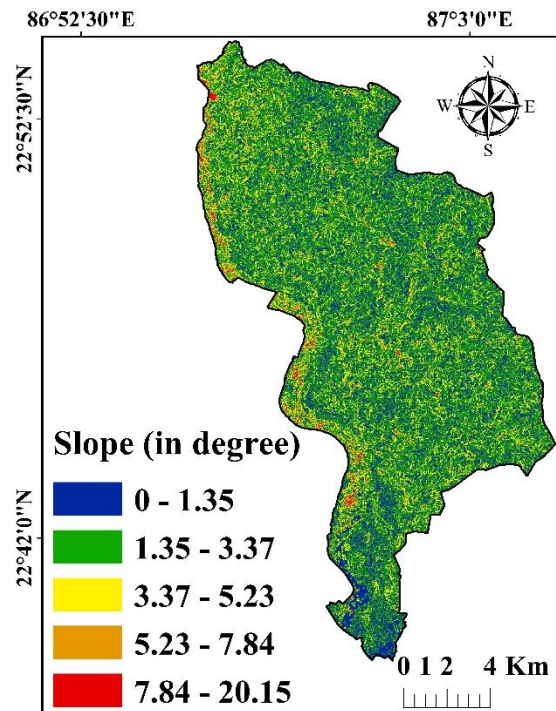

Figure 12. Slope map.

Steeper slopes accelerate runoff, reducing groundwater recharge time. In contrast, gentler

slopes slow water infiltration, enhancing groundwater recharge [61-62]. Slope angles (º) were derived from ALOS PALSAR DEM data using QGIS. The area is classified into five slope categories shown in Figure 12. Places with slope of 0 - 1.35 degree (27.2 percent) has been considered excellent, 1.35 - 3.37 degree (52.9 percent) and 3.37 - 5.23 degree (15.7 percent) as good, while 5.23 - 7.84 degree (3.5 percent) and 7.84 - 20.15 degrees (0.7 percent) have been considered as fair potential zone.

3.9 Topographic Wetness Index (TWI)

The topography of an area has a significant impact on the movement of water, and it's distributed across the landforms. Steep slope led to faster surface runoff, reducing the infiltration rate and limiting the amount of water that replenishes underground aquifers. On the other hand, gentle slopes encourage water to seep into the soil, effectively recharging aquifers. The Topographic Wetness Index (TWI) indicates how the topography becomes saturated. High TWI values suggest the topography is already water-saturated and generates more runoff due to saturation excess, influencing areas prone to water accumulation and higher soil moisture, thereby enhancing groundwater recharge [63-65].
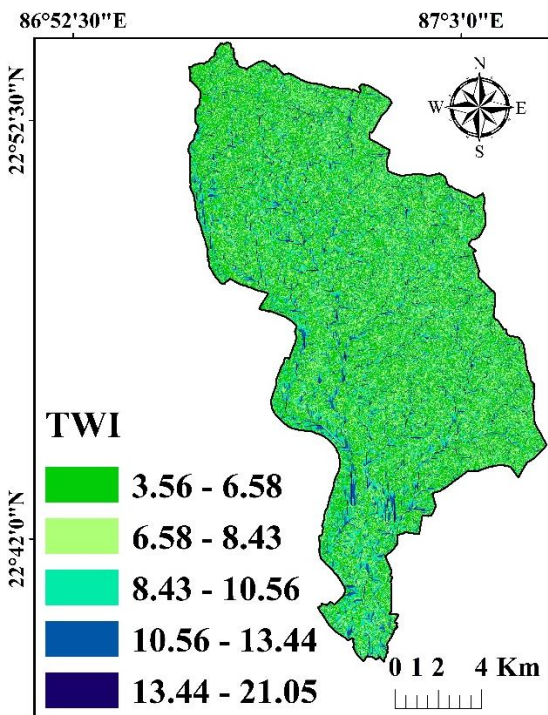

Figure 13. TWI map.

Lower TWI values indicate lower GWP, while higher values suggest greater potential [66-67]. The study area was classified into five TWI classes, specifically 3.56 - 6.58 (41%) 6.58 - 8.43 (29%) with fair GWP, 8.43 - 10.56 (20.6%) with good, and 10.56 - 13.44 (7.4%) and 13.44 - 21.05 (2%) with excellent GWP given in Figure 13.

3.10 Soil Texture (ST)

Soil texture is an important element that determines the rate of infiltration, surface runoff, porosity, and permeability and aids in defining the appropriate GWP. Soil with coarser textures such as sandy loam facilitate higher infiltration rate and groundwater recharge compared to finer textures like clay loam, having lower infiltration capability and may impede recharge [29]. Soil texture classes also affect water holding capacity of soil, influencing the availability of water for groundwater replenishment during dry periods [25]. Therefore, the soil texture classes were translated into GWP ranks based on their permeability and infiltration characteristics. For example, sandy loam to clay loam–gravelly sandy clay was assigned a rank of 8 (excellent) due to its high porosity and infiltration capacity, which facilitates effective groundwater recharge. In contrast, clay loam to clay–clay, with low permeability and high runoff potential, was assigned a rank of 4 (fair). This ranking approach aligns with established hydrological principles and similar groundwater studies in semi-arid regions [25,29]. The soil texture classes of the study area significantly influence GWP. Zones with waterbodies (4.5%), sandy loamy sand to sandy loam (10.7%), and sandy loam to clay loam - gravelly sandy clay (25.6%) have excellent GWP due to high permeability and infiltration rates.
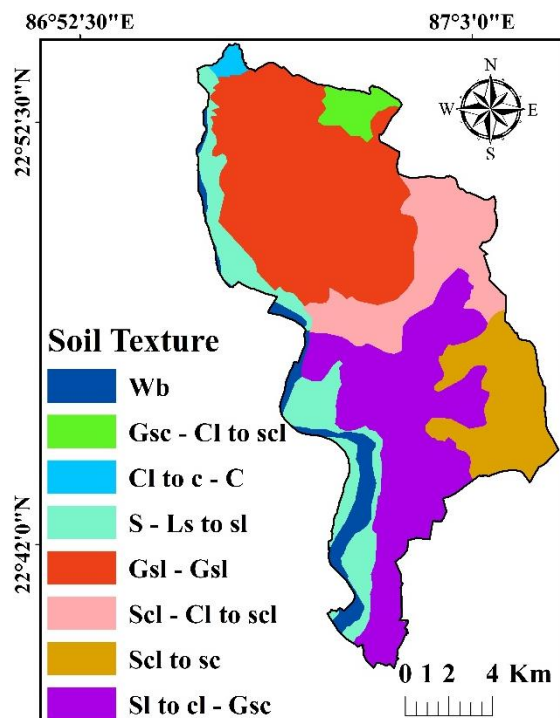

Figure 14. Soil texture map (**Wb**-Water bodies, **Gsc**-Gravelly sandy clay, **Cl**-Clay loam, **Scl**-Sandy clay loam, **C**-clay, **S**-Sandy, **Ls**-Loamy sand, **Sl**-Sandy loam **Gsl**-Gravelly sandy loam, **Sc**-Sandy clay).

Where, Gravelly sandy loam to gravelly sandy loam (32.7%) and sandy clay loam - clay loam to sandy clay loam (12.5%) have good prospect.

Furthermore, gravelly sandy clay - clay loam to sandy clay loam (2.3%), clay loam to clay-clay (0.7%), and sandy clay loam to sandy clay (11.0%) offer fair GWP due to lower permeability (Figure 14).

3.11   Comparison of GWP in AHP, MIF, and RF

The three methods, AHP, MIF, and RF, have been used for producing GWP for the study area. For this purpose, all the thematic layers were converted into raster format with the same cell size and finally reclassified for their processing. Finally, the datasets were overlaid using the weighted overlay and ML algorithm for GWP demarcation. The GWP maps resulting from the above methods were classified into four main categories based on the availability of groundwater, namely poor, fair, good, and excellent. There are multiple studies that utilized a similar kind of classification for GWP zonation [15,46]. The class with the lowest GWP has poor potential, while the class with optimum groundwater availability was referred as excellent. The categorisation of the groundwater (GW) yield data has also been done accordingly to match the GWP with the actual classification given in the GW prospect dataset. The spatial distribution of various GWP is presented in Table 4.

Table 4. Percentage (%) wise groundwater classes in AHP, MIF and RF

Type	GW yield (lpm)	GWP	AHP (%)	MIF (%)	RF (%)
1	30 – 50	Poor	22	15	23
2	50 – 100	Fair	38	42	47
3	100 – 400	Good	35	36	25
4	400 – 800	Excellent	5	7	5

The study's findings from all the used methods indicated that the northern and eastern regions, characterized by sandy lateritic formations, low lineament, and drainage density, a lower water table, relatively less rainfall, and high vegetation cover, demonstrate poor to fair GWP, with minimal influence from slope and TWI. In contrast, the eastern, southern, and central regions show fair to excellent potential. This is due to the presence of clayey alluvial formations, high lineament and drainage density, a higher water table, sufficient rainfall, and extensive agricultural lands. The effects of slope and TWI are observed to be minimal.

For the AHP method, the CI (0.128), RI (1.51), and CR (0.085) value obtained using equations 5 and 6 were satisfactory as it lower than its desired upper limit of 0.10. These values and the value of λmax (12.282) were determineded using a self-developed MS Excel sheet-based AHP weightage calculator created by combining equations, for the total number of variables (n). Using the AHP method in the present study, a total of four GWP zones were found (Figure 15.).
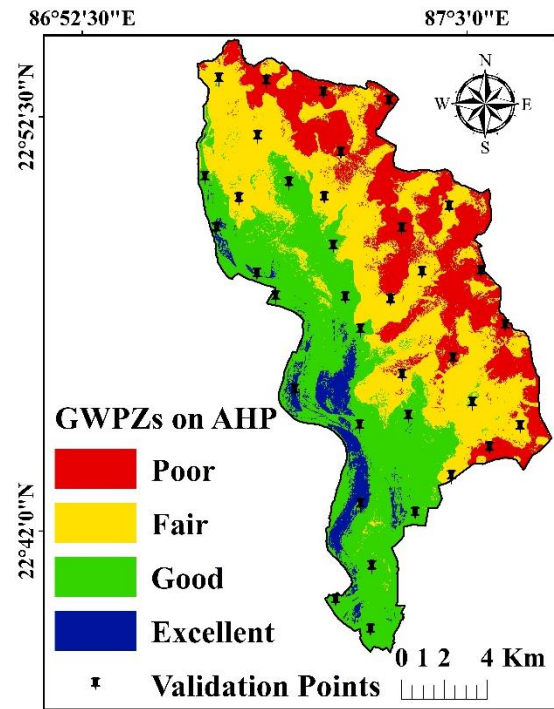

Figure 15. GWP zones on AHP method.

These zones are marked according to their GWP from poor to excellent. The result of the work revealed that about 22 % of the total study area has poor GWP, 38 % of the area has fair, 35 % of the area has good, and only about 5 % of the remaining area has excellent GWP.
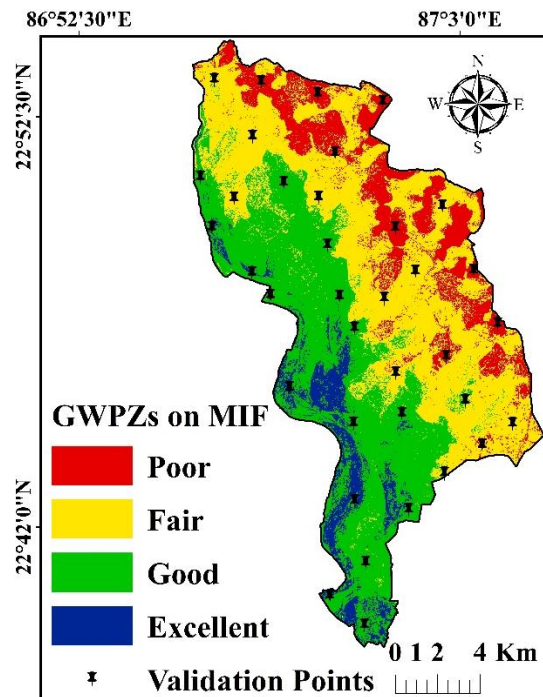

Figure 16. GWP zones on MIF method.

The MIF method also has successfully delineated the GWP in the present study. As a result, four groundwater prospect zones were identified and categorized from poor to excellent as shown in Figure 16. About 15 % and 42 % of the area poor and fair GWP while 36 % and 7 % of the total study area

recognized with good and excellent GWP, respectively.

The GWP obtained from the RF algorithm have also produced outstanding result as compared to the traditional methods, which were further categorized into four GWP groups, namely poor, fair, good, and excellent. Almost 23 % of the study area accounts for poor GWP, the fair zone is extended over 47 % of the area, the good GWP covers 25 % of the area, and the excellent GWP covers 6 % of the study area respectively, as shown in Figure 17.
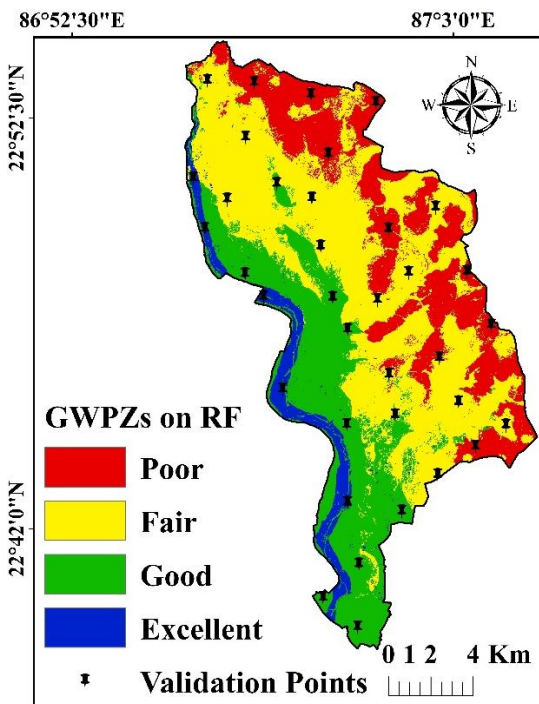

Figure 17. GWP zones on RF method.

The model was tuned using GridSearchCV, to identify the optimal parameters namely max_depth as None, min_samples_leaf as 1, min_samples_split as 2, and n_estimators as 200 [36]. The cross-validation's result shows an overall accuracy of 78%, where the precision, recall, and f1-scores for groundwater potential classes have been obtained as 0.83,1.00 and 0.91 for class 0 (excellent), 0.71, 0.45, and 0.56 for class 1 (good), 0.64, 0.82 and 0.72 for class 2 (fair), and 1.00, 1.00 and 1.00 for class 3 (poor). The model has efficiently predicted GWP of the study area and generated an ROC curve with a macro-average Area Under the Curve (AUC,) which indicates a good performance and provided valuable insights for groundwater resource management.

3.11.1 Statistical comparison of GWP

The Chi-square goodness of fit and Mann-Whitney tests have been conducted to compare the efficacy of GWP maps prepared using the aforementioned methods. Both the tests were carried out by comparing the model output GWP maps (predicted) with that of GWP identified using field observation on groundwater yield (lpm) data of

NRSC ISRO and collected from West Bengal Public Health Engineering Department (WBPHED) (observed).

Chi-square test evaluates differences between predicted/observed and expected frequencies in the GWP mapping by various models. A significant difference between observed and expected frequencies indicates a discrepancy, suggesting the need for further investigation or model adjustment [68].
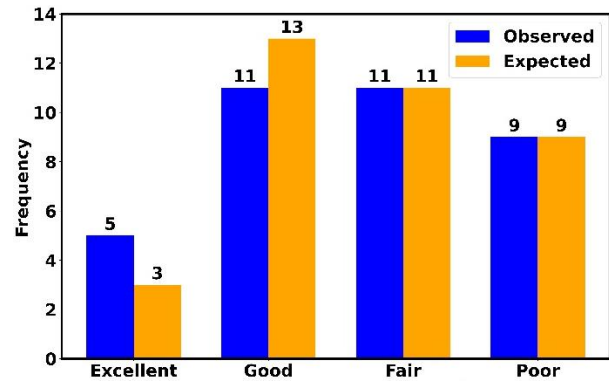

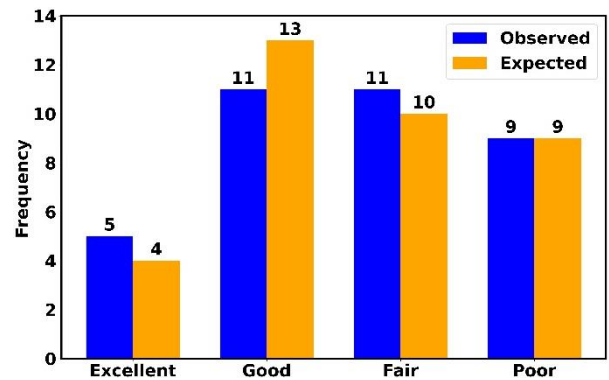**Figure 18.** Chi-square goodness of fit result for AHP.

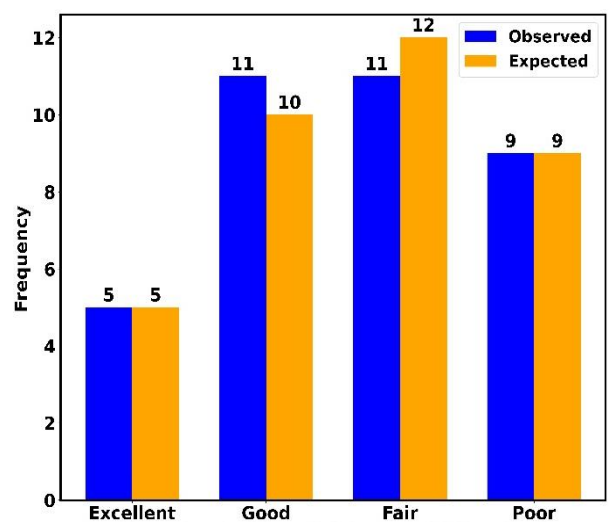**Figure 19.** Chi-square goodness of fit result for MIF.

Figure 20. Chi-square goodness of fit result for RF.

In the AHP method, the chi-square statistic (1.641) is less than the critical value (7.815), and the p-value (0.650) is greater than 0.05, indicates a match between observed and expected frequencies.

While MIF method also showed identical result with a chi-square statistic of 0.658 and a p-value of 0.883. On the contrary, the RF method with a chi-square value of 0.183 and a high p-value of 0.980, suggests that the observed frequencies match expected frequencies [69]. The p-values indicates that the results obtained using RF is more strongly confirming the null hypothesis (Figure 18 - 20).

The Mann-Whitney U test, a non-parametric test, was applied to compare the GWP classifications from three Multi-Criterion Decision-Making (MCDM) methods namely AHP, MIF, and RF against the ground truth values.
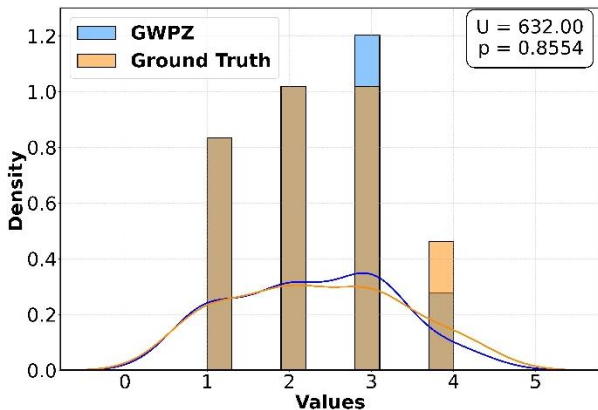

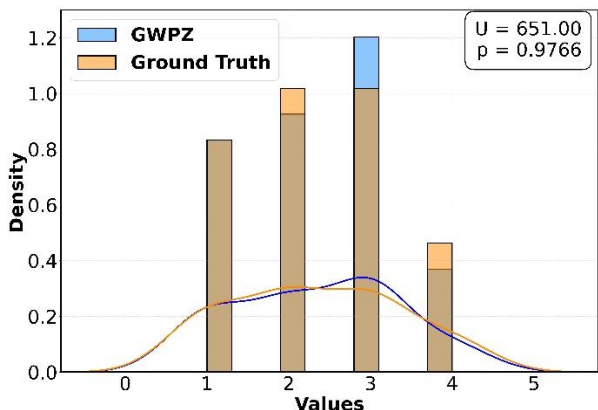**Figure 21.** Mann-Whitney U test results for AHP.

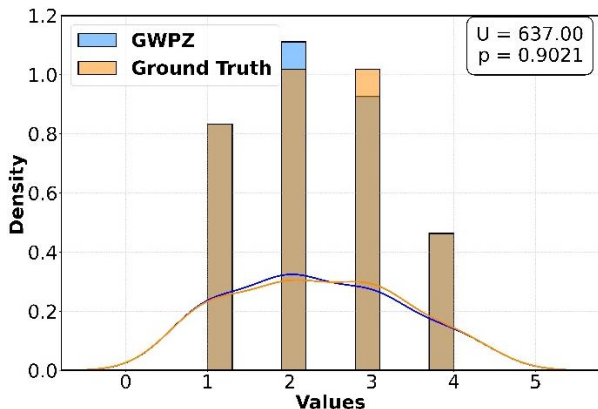**Figure 22.** Mann-Whitney U test results for MIF.

Figure 23. Mann-Whitney U test results for RF.

This test, which compares the ranks of two independent groups, is beneficial when the data does not follow a normal distribution [70]. The p-values

for all three methods (AHP: 0.8554, MIF: 0.9766, and RF: 0.9021) were all greater than 0.05, indicating no significant differences between the predicted GWP values and the ground truth. Among the methods, MIF showed the highest U statistic value (651.0), suggesting a slightly better ranking; however, the difference was not statistically significant. Overall, the results indicate that all three methods perform similarly when evaluated using the Mann-Whitney U test (Figure 21 - 23). This aligns with the idea that non-parametric tests like Mann-Whitney are valuable for comparing non-normally distributed data without assuming a specific underlying distribution. Hence, these outcomes implied that the AHP, MIF, and RF methods offer efficient and dependable prediction of GWP concerning the observed groundwater yield data from WBPHED.

4. Valıdatıon of GWP zonation Maps

The present study adopted three methodologies (AHP, MIF, and RF) to delineate GWP and used the mean macro-average Receiver Operating Characteristic (ROC) Area Under the Curve (AUC) for validation of the result. This method evaluates an overall evaluation of the model's performance across all classes and is particularly useful for assessing multi-class classifiers [36,71]. Groundwater yield data has been used to validate the potential zones across 36 random points taken for model validation after consulting a local geologist. The total number of validation points to be used in this work was finalized after a rigorous literature survey, where a study used 14 observation wells for GWP validation for an area of 976 km^2, another two studies used 12 and 32 observation wells for validating 847 km^2 and 3149 km^2 study areas, respectively [15,46,48].

During the validation process, it has been found that the AHP method achieved a mean macro-average ROC AUC of 0.875, and MIF achieved 0.828 AUC, where RF performed exceptionally well with an AUC score of 0.982 (Figure 24 - 26).
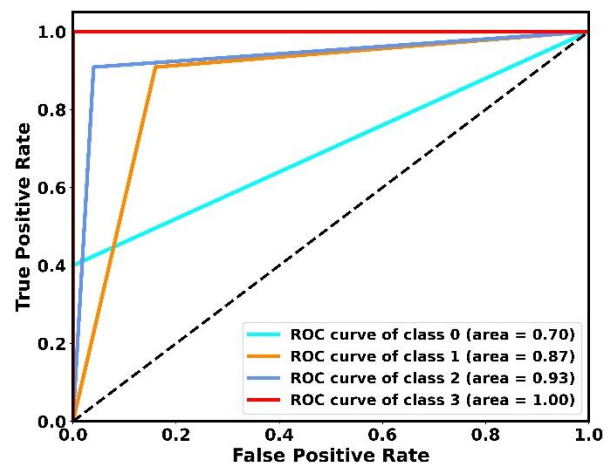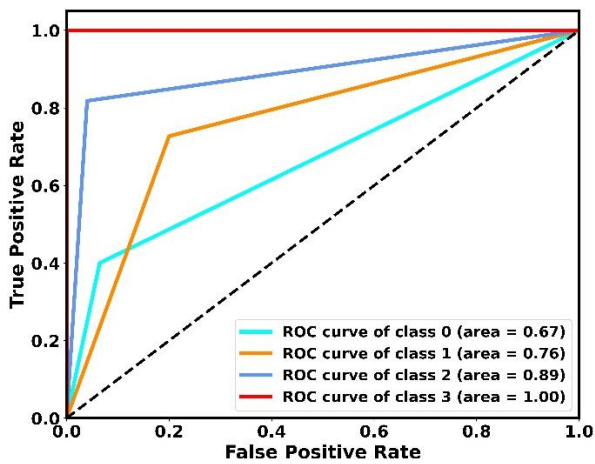

Figure 24. AHP ROC curve.
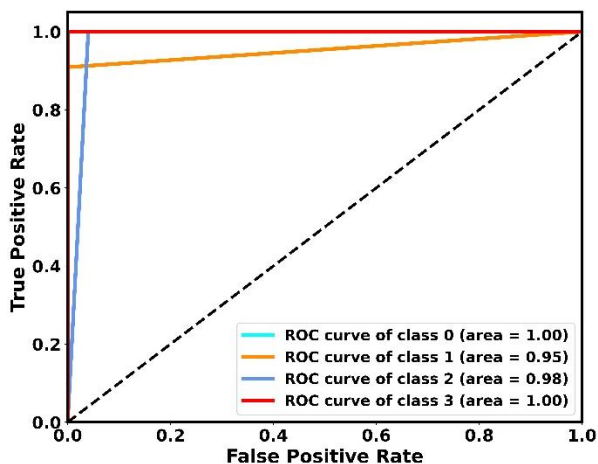
Figure 25. MIF ROC curve.

Figure 26. RF ROC curve.

This indicates that the RF model has a higher prediction accuracy compared to AHP and MIF in delineating GWP within the study area, proclaiming its robustness and reliability for hydrogeological applications.

These findings provide invaluable insights for policymakers and local communities to implement targeted interventions, such as rainwater harvesting, artificial recharge, and efficient irrigation practices. However, the incorporating time-series data to assess changes in groundwater potential over time, collaborating with local communities to co-develop groundwater management strategies and developing advanced models to predict future trends in groundwater availability and quality will help in better achieving the groundwater sustainability in the region.

5. Conclusıon

The present work to decipher the GWP of the Sarenga block of Bankura district, West Bengal has efficiently handled and evaluated, how the implementation of GIS and RS coupled with MCDM techniques can lead to the successful delineation of the GWP. The study unveils that out of the eleven factors used in the study, geomorphology, geology, drainage, and lineament have the highest impact on the GWP.

The GWP maps obtained using the aforementioned models were compared using the Chi-square test and Mann-Whitney tests, which showed the edge of the RF model as compared to the other two methods. The validation results of ROC AUC foreclosed that the RF model produced an AUC of 0.982, outperforming AHP's 0.875 and MIF's 0.828. Thus, the study concludes that the machine learning-based RF model is more effective than the traditional AHP and MIF methods for delineating GWP in regions with similar geographical settings, suggesting future studies may explore advanced ML models such as XGBoost, Support Vector Machines (SVM), or Gradient Boosting, which are capable of capturing more complex hydrogeological patterns. The model performance can also be improved with proper tuning, including a larger number of ground truth points, and implementing a more efficient quantitative data handling strategy.

The RF model has depicted that 23 % and 47% of the area exhibits poor and fair GWP. While, about 25% and 5% of the study area have good and excellent GWP. The study suggests that the south and western parts of the region have excellent to good groundwater potential, while the north and eastern parts have fair to poor GWP. On the contrary, the central part has fair to good GWP. Though the study identifies the zones of GW scarcity and adequacy, it also recommends promoting rainwater collection and building storage and recharge facilities in areas with poor groundwater potential to improve GWP. Finally, it also advocates for regular monitoring of groundwater to plan its sustainable usage for agricultural applications using GIS and RS, and encourage local integrated groundwater management.

This work acknowledges certain limitations, including the DEM-related errors, the availability of fewer rainfall stations, coarse-scale geology and soil data, and the use of a single-year groundwater database. While these are quite common in GIS-based hydrogeological studies, they were minimized with data standardization and validation. Future work should incorporate multi-temporal datasets and more adequate field observation data to further improve reliability.

Author Contributions

Suraj Dule: Data collection, Methodology, Validation, Resources, Formal analysis,

Investigation, Writing-Original draft preparation
Arabinda Sharma: Conceptualization, Methodology, Resources, Supervision, Reviewing and editing.

Conflicts of Interest

The authors declare that they have no known competing financial and non-financial interests or personal relationships that could have appeared to influence the work reported in this paper.

References

1. Hussain, S., & Mahmood, S. (2023). Analyzing Domestic Water Consumption in Wana, South Waziristan, Khyber Pakhtunkhwa Province- Pakistan. Advanced Geomatics, 3(1), 16-22.

2. Ünel, F. B., Kuşak, L., Yakar, M., & Doğan, H. (2023). Coğrafi bilgi sistemleri ve analitik hiyerarşi prosesi kullanarak Mersin ilinde otomatik meteoroloji gözlem istasyonu yer seçimi. Geomatik, 8(2), 107-123.

3. Kinzelbach, W., Bauer, P., Siegfried, T., & Brunner, P. (2003). Sustainable groundwater management—problems and scientific tools. Episodes Journal of International Geoscience, 26(4), 279-284.

4. Berhanu, K. G., & Hatiye, S. D. (2020). Identification of groundwater potential zones using proxy data: case study of Megech Watershed, Ethiopia. Journal of Hydrology: Regional Studies, 28, 100676.

5. Das, S. (2017). Delineation of groundwater potential zone in hard rock terrain in Gangajalghati block, Bankura district, India using remote sensing and GIS techniques. Modeling Earth Systems and Environment, 3(4), 1589-1599.

6. Waikar, M. L., & Nilawar, A. P. (2014). Identification of groundwater potential zone using remote sensing and GIS technique. International Journal of Innovative Research in Science, Engineering and Technology, 3(5), 12163-12174.

7. Patil, R., & Datta, M. (2022). Spatio-Temporal Analysis of Climate Change in India: a Theoretical Perspective. Advanced Geomatics, 2(1), 07-13.

8. Jamil, M., Mahmood, S., Husssain, S., & Saad, M. (2024). Assessing the impact of drought on groundwater resources using geospatial techniques in Balochistan Province, Pakistan. Advanced Remote Sensing, 4(1), 11-27.

9. Ahirwar, R., Malik, M. S., Ahirwar, S., & Shukla, J. P. (2021). Groundwater potential zone mapping of Hoshangabad and Budhni industrial area, Madhya Pradesh, India. Groundwater for Sustainable Development, 14, 100631.

10. Makhmudov, R., & Teymurov, M. (2024). Importance of using GIS software in the process of application of Analogue terrains and Counter-approach technologies in water resources assessment. Advanced Remote Sensing, 4(1), 36-45.

11. Avtar, R., Singh, C. K., Shashtri, S., Singh, A., & Mukherjee, S. (2010). Identification and analysis of groundwater potential zones in Ken–Betwa river linking area using remote sensing and geographic information system. Geocarto International, 25(5), 379-396.

12. Memduhoglu, A. (2023). Identifying impervious surfaces for rainwater harvesting feasibility using unmanned aerial vehicle imagery and machine learning classification. Advanced GIS, 3(1), 01-06.

13. Najatishendi, E., Ergene, E. M., Uzar, M., & Şanlı, F. B. (2022). Production of flood risk maps: Ayancık Stream Example. Mersin Photogrammetry Journal, 4(1), 24-31.

14. Pande, C. B., Moharir, K. N., Panneerselvam, B., Singh, S. K., Elbeltagi, A., Pham, Q. B., & Rajesh, J. (2021). Delineation of groundwater potential zones for sustainable development and planning using analytical hierarchy process (AHP), and MIF techniques. Applied Water Science, 11(12), 186.

15. Patra, S., Mishra, P., & Mahapatra, S. C. (2018). Delineation of groundwater potential zone for sustainable development: A case study from Ganga Alluvial Plain covering Hooghly district of India using remote sensing, geographic information system and analytic hierarchy process. Journal of Cleaner Production, 172, 2485-2502.

16. Yadav, B., Malav, L. C., Jangir, A., Kharia, S. K., Singh, S. V., Yeasin, M., & Yadav, K. K. (2023). Application of analytical hierarchical process, multi-influencing factor, and geospatial techniques for groundwater potential zonation in a semi-arid region of western India. Journal of Contaminant Hydrology, 253, 104122.

17. Öcül, M., & Şişman, A. (2023). Landslide susceptibility analysis with multi criteria decision methods; a case study of Taşova. Advanced GIS, 3(1), 14–21. Retrieved from https://publish.mersin.edu.tr/index.php/agis/article/view/835

18. Das, S., Gupta, A., & Ghosh, S. (2017). Exploring groundwater potential zones using MIF technique in semi-arid region: a case study of Hingoli district, Maharashtra. Spatial Information Research, 25, 749-756.

19. Saravanan, S., Saranya, T., & Abijith, D. (2022). Application of frequency ratio,

analytical hierarchy process, and multi-influencing factor methods for delineating groundwater potential zones. International Journal of Environmental Science and Technology, 19(12), 12211-12234.

20. Thanh, N. N., Chotpantarat, S., Trung, N. H., & Ngu, N. H. (2022). Mapping groundwater potential zones in Kanchanaburi Province, Thailand by integrating of analytic hierarchy process, frequency ratio, and random forest. Ecological Indicators, 145, 109591.

21. Masroor, M., Rehman, S., Sajjad, H., Rahaman, M. H., Sahana, M., Ahmed, R., & Singh, R. (2021). Assessing the impact of drought conditions on groundwater potential in Godavari Middle Sub-Basin, India using analytical hierarchy process and random forest machine learning algorithm. Groundwater for sustainable development, 13, 100554.

22. Roy, P., Pal, S. C., Chakrabortty, R., Chowdhuri, I., Saha, A., & Shit, M. (2022). Climate change and groundwater overdraft impacts on agricultural drought in India: Vulnerability assessment, food security measures and policy recommendation. Science of the total environment, 849, 157850.

23. Das, S. (2019). Comparison among influencing factor, frequency ratio, and analytical hierarchy process techniques for groundwater potential zonation in Vaitarna basin, Maharashtra, India. Groundwater for Sustainable Development, 8, 617-629.

24. Khosravi, K., Sartaj, M., Tsai, F. T. C., Singh, V. P., Kazakis, N., Melesse, A. M., & Pham, B. T. (2018). A comparison study of DRASTIC methods with various objective methods for groundwater vulnerability assessment. Science of the total environment, 642, 1032-1049.

25. Chowdhury, A., Jha, M. K., Chowdary, V. M., & Mal, B. C. (2009). Integrated remote sensing and GIS-based approach for assessing groundwater potential in West Medinipur district, West Bengal, India. International Journal of Remote Sensing, 30(1), 231-250.

26. Rahmati, O., Pourghasemi, H. R., & Melesse, A. M. (2016). Application of GIS-based data driven random forest and maximum entropy models for groundwater potential mapping: a case study at Mehran Region, Iran. Catena, 137, 360-372.

27. Nag, S. K., Chowdhury, P., Das, S., & Mukherjee, A. (2021). Deciphering prospective groundwater zones in Bankura district, West Bengal: a study using GIS platform and MIF techniques. International Journal of Energy and Water Resources, 5, 323-341.

28. Sahu, B. B., & Kumar, A. (2022). Aquifer Mapping and Management of Ground Water Resources Bankura District West Bengal. https://www.cgwb.gov.in/cgwbpnm/public/uploads/documents/16905335181706431115file.pdf

29. Abate, S. G., Amare, G. Z., & Adal, A. M. (2022). Geospatial analysis for the identification and mapping of groundwater potential zones using RS and GIS at Eastern Gojjam, Ethiopia. Groundwater for Sustainable Development, 19, 100824.

30. Saranya, T., & Saravanan, S. (2020). Groundwater potential zone mapping using analytical hierarchy process (AHP) and GIS for Kancheepuram District, Tamilnadu, India. Modeling Earth Systems and Environment, 6(2), 1105-1122.

31. Çitfçi, H., & KUŞAK, L. (2021). Determination of unsuitability points on the route of Van Gölü-Kapıköy railway line by using GIS and AHP method. Advanced GIS, 1(1), 27–37. Retrieved from https://publish.mersin.edu.tr/index.php/agis/article/view/69

32. Saaty, T. L. (2008). Decision making with the analytic hierarchy process. International journal of services sciences, 1(1), 83-98.

33. Breiman, L. (2001). Random forests. Machine learning, 45, 5-32.

34. Liaw, A., & Wiener, M. (2002). Classification and regression by randomForest. R news, 2(3), 18-22.

35. Cutler, D. R., Edwards Jr, T. C., Beard, K. H., Cutler, A., Hess, K. T., Gibson, J., & Lawler, J. J. (2007). Random forests for classification in ecology. Ecology, 88(11), 2783-2792.

36. Svetnik, V., Liaw, A., Tong, C., Culberson, J. C., Sheridan, R. P., & Feuston, B. P. (2003). Random forest: a classification and regression tool for compound classification and QSAR modeling. Journal of chemical information and computer sciences, 43(6), 1947-1958.

37. Ayalke, G. Z., & Şişman, A. (2024). Google Earth Engine kullanılarak makine öğrenmesi tabanlı iyileştirilmiş arazi örtüsü sınıflandırması: Atakum, Samsun örneği. Geomatik, 9 (3), 375-390.

38. Özdemir, E. G., Zengin, T. U., & Güleç, H. A. (2024). Orman ekosistemindeki ağaç boylarının, optik, radar, lazer altimetre uydu verileri ve yardımcı kaynaklar kullanılarak Google Earth Engine platformunda modellenmesi. Geomatik, 9 (2), 259-268.

39. Todd, D. K., & Mays, L. W. (2004). Groundwater hydrology. John Wiley & Sons.

40. Thapa, R., Gupta, S., Guin, S., & Kaur, H. (2017). Assessment of groundwater potential zones using multi-influencing factor (MIF) and GIS: a case study from

Birbhum district, West Bengal. Applied Water Science, 7, 4117-4131.

41. Gessler, P. E., Moore, I. D., McKenzie, N. J., & Ryan, P. J. (1995). Soil-landscape modelling and spatial prediction of soil attributes. International journal of geographical information systems, 9(4), 421-432.

42. Shaban, A., Khawlie, M., & Abdallah, C. (2006). Use of remote sensing and GIS to determine recharge potential zones: the case of Occidental Lebanon. Hydrogeology Journal, 14, 433-443.

43. Karakoca, E., & Ünver, A. (2025). Analitik Hiyerarşi Süreci ve Coğrafi Bilgi Sistemleri Kullanarak Eşen Çay Havzası'nda Taşkın Riski Değerlendirmesi ve Haritalandırılması. Geomatik, 10 (1), 127-143

44. Anderson, M. P., Woessner, W. W., & Hunt, R. J. (2015). Applied groundwater modeling: simulation of flow and advective transport. Academic press.

45. Freeze, R. A., & Cherry, J. A. (1979). Groundwater prentice-hall. Englewood Cliffs, NJ, 176, 161-177.

46. Achu, A. L., Thomas, J., & Reghunath, R. (2020). Multi-criteria decision analysis for delineation of groundwater potential zones in a tropical river basin using remote sensing, GIS and analytical hierarchy process (AHP). Groundwater for Sustainable Development, 10, 100365.

47. Çelik, M. Ö., Kuşak, L., & Yakar, M. (2024). Assessment of groundwater potential zones utilizing geographic information system-based analytical hierarchy process, Vlse Kriterijumska Optimizacija Kompromisno Resenje, and technique for order preference by similarity to ideal solution methods: a case study in Mersin, Türkiye. Sustainability, 16(5), 2202.

48. Arunbose, S., Srinivas, Y., Rajkumar, S., Nair, N. C., & Kaliraj, S. (2021). Remote sensing, GIS and AHP techniques based investigation of groundwater potential zones in the Karumeniyar river basin, Tamil Nadu, southern India. Groundwater for Sustainable Development, 14, 100586.

49. Ganapuram, S., Kumar, G. V., Krishna, I. M., Kahya, E., & Demirel, M. C. (2009). Mapping of groundwater potential zones in the Musi basin using remote sensing data and GIS. Advances in Engineering Software, 40(7), 506-518.

50. Ergene, E. M., Najatishendi, E., Uzar, M., & Şanlı, F. B. (2022). Determination of Ayancık Stream Basin and its morphometric parameters. Mersin Photogrammetry Journal, 4(1), 14-23.

51. Horton, R. E. (1945). Erosional development of streams and their drainage basins;

hydrophysical approach to quantitative morphology. Geological society of America bulletin, 56(3), 275-370.

52. Rahmati, O., Nazari Samani, A., Mahdavi, M., Pourghasemi, H. R., & Zeinivand, H. (2015). Groundwater potential mapping at Kurdistan region of Iran using analytic hierarchy process and GIS. Arabian Journal of Geosciences, 8, 7059-7071.

53. Scanlon, B. R., Healy, R. W., & Cook, P. G. (2002). Choosing appropriate techniques for quantifying groundwater recharge. Hydrogeology journal, 10, 18-39.

54. Pai, D. S., Rajeevan, M., Sreejith, O. P., Mukhopadhyay, B., & Satbha, N. S. (2014). Development of a new high spatial resolution (0.25× 0.25) long period (1901-2010) daily gridded rainfall data set over India and its comparison with existing data sets over the region. Mausam, 65(1), 1-18.

55. Bag, A., Sharma, A., & Pal, S. (2024). Studying urbanization pattern in Sambalpur City during 1992-2042 using CA-ANN, and Markov-Chain model. International Journal of Engineering and Geosciences, 9(3), 356-367.

56. Rwanga, S. S., & Ndambuki, J. M. (2017). Accuracy assessment of land use/land cover classification using remote sensing and GIS. International Journal of Geosciences, 8(04), 611.

57. Tewabe, D., & Fentahun, T. (2020). Assessing land use and land cover change detection using remote sensing in the Lake Tana Basin, Northwest Ethiopia. Cogent Environmental Science, 6(1), 1778998.

58. Yakar M, Yılmaz H M & Mutluoğlu Ö (2010). Comparative evaluation of excavation volume by TLS and total topographic station based methods. Lasers in Eng,19, 331-345..

59. Yakar, M., Yilmaz, H. M., & Yurt, K. (2010). The effect of grid resolution in defining terrain surface. Experimental Techniques, 34(6), 23-29.

60. Gull, A., Liaqu, A., & Mahmood, S. (2023). Landslide Risk Assessment using Geo-spatial Technique: A study of District Abbottabad, Khyber Pakhtunkhwa, Pakistan. Advanced Geomatics, 3(2), 47-55.

61. Raj, S., Rawat, K. S., Singh, S. K., & Mishra, A. K. (2024). Groundwater potential zones identification and validation in Peninsular India. Geology, Ecology, and Landscapes, 8(1), 86-100.

62. Yakar, M. (2011). Using close range photogrammetry to measure the position of inaccessible geological features. Experimental Techniques, 35(1), 54-59..

63. Kopecký, M., Macek, M., & Wild, J. (2021). Topographic Wetness Index calculation guidelines based on measured soil moisture

and plant species composition. Science of the Total Environment, 757, 143785.

64. Pandian, R. S., Udayakumar, S., Balaji, K. K. P., & Narayanan, R. L. (2023). Identification of groundwater potential for urban development using multi-criteria decision-making method of analytical hierarchy process. International Journal of Engineering and Geosciences, 8(3), 318-328.

65. Sörensen, R., Zinko, U., & Seibert, J. (2006). On the calculation of the topographic wetness index: evaluation of different methods based on field observations. Hydrology and Earth System Sciences, 10(1), 101-112.

66. Beven, K. J., & Kirkby, M. J. (1979). A physically based, variable contributing area model of basin hydrology/Un modèle à base physique de zone d'appel variable de l'hydrologie du bassin versant. Hydrological sciences journal, 24(1), 43-69.

67. Sharma, A. (2010) Integrating Terrain and Vegetation Indices for Identifying Erosion Risk Area. Geo-spatial Information Science, 13 (3), 201-209. https://doi.org/10.1007/s11806-010-0342-6

68. Agresti, A. (2013). Categorical data analysis. John Wiley & Sons.

69. McHugh, M. L. (2013). The chi-square test of independence. Biochemia medica, 23(2), 143-149.

70. Mann, H. B., & Whitney, D. R. (1947). On a test of whether one of two random variables is stochastically larger than the other. The annals of mathematical statistics, 50-60.

71. Fawcett, T. (2006). An introduction to ROC analysis. Pattern recognition letters, 27(8), 861-874.